1521-0103/381/3/257–265$35.00
THE JOURNAL OF PHARMACOLOGY AND EXPERIMENTAL THERAPEUTICS

dx.doi.org/10.1124/jpet.121.001020
J Pharmacol Exp Ther 381:257–265, June 2022

Ligustrazine Attenuates Liver Fibrosis by Targeting miR-145 Mediated Transforming Growth Factor-β/Smad Signaling in an Animal Model of Biliary Atresia

Jian-Li Qiu,[1] Guo-Feng Zhang,[1] Yu-Na Chai, Xiao-Yan Han, Hai-Tao Zheng, Xiang-Feng Li, Fei Duan and Ling-Yan Chen

Department of Pediatrics (J.-L.Q., H.-T.Z., X.-F.L.) and Department of Gastroenterology (F.D.), the First Affiliated Hospital of Henan University of Chinese Medicine, Zhengzhou, China; Department of Pediatric Surgery (G.-F.Z.) and Department of Pharmacy (Y.-N.C.), the First Affiliated Hospital of Zhengzhou University, Zhengzhou, China; Henan University of Chinese Medicine, Zhengzhou, China (X.-Y.H.); and Department of Rehabilitation, the First Affiliated Hospital of Guangzhou Medical University, Guangzhou, China (L.-Y.C.)

Received November 15, 2021; accepted March 28, 2022

ABSTRACT

To investigate therapeutic target for ligustrazine during liver fibrosis in an ethanol-induced biliary atresia rat model and transforming growth factor-β (TGF-β) induced hepatic stellate cell activation cell model, and the underlying mechanism, a total of 30 rats were randomly assigned into five groups ($n = 6$ per group): control, sham, ethanol-induced biliary atresia model, model plus pirfenidone, and model plus ligustrazine groups. The liver changes were assessed using H&E and Masson staining and transmission electron microscopy. Expression of miR-145 and mRNA and protein levels of TGF-β/smads pathway-related proteins were detected. HSC-T6 cells were infected with LV-miR or rLV-miR-145 in the presence or absence of SMAD3 inhibitor SIS3 and treated with 2.5 ng/ml TGF-β1 and then with ligustrazine. Collected cells were subjected to detect the expression of miR-145 and mRNA and protein expression levels of TGF-β/smads pathway–related proteins. Ligustrazine rescued liver fibrogenesis and pathology for ethanol-caused bile duct injury, revealed by decreased α-smooth muscle actin and collagen I expression and liver tissue and cell morphology integrity. Further experiments showed that ligustrazine inhibited intrinsic and phosphorylated Smad2/3 protein expression and modification. Similar results were obtained in cells. In addition, ligustrazine altered miR-145 expression in both animal and cell models. Lentivirus mediated miR-145 overexpression and knockdown recombinant virus showed that miR-145 enhanced the TGF-β/Smad pathway, which led to hepatic stellate cell activation, and ligustrazine blocked this activation. This work validated that ligustrazine-regulated miR-145 mediated TGF-β/Smad signaling to inhibit the progression of liver fibrosis in a biliary atresia rat model and provided a new therapeutic strategy for liver fibrosis.

SIGNIFICANCE STATEMENT

With an ethanol-induced biliary atresia rat model, ligustrazine was found to rescue liver fibrogenesis and pathology for ethanol caused bile duct injury, revealed by decreased α-smooth muscle actin and collagen I expression and liver tissue and cell morphology integrity. Furthermore, we found ligustrazine upregulated miR-145 expression and inhibited TGF-β/SMAD signaling pathway both in vivo and in vitro. In addition, overexpression and knockdown of miR-145 confirmed that miR-145 is involved in the ligustrazine inhibition of liver fibrosis through the TGF-β/SMAD signaling pathway.

Introduction

Biliary atresia is a leading cause of neonatal cholestasis that results from an inflammatory and fibrosing obstruction of extrahepatic bile ducts. Biliary atresia rapidly progresses to end-stage cirrhosis, leading to high mortality in children (Govindarajan, 2016). The disease occurs with different geographical frequencies with approximately 1 in 15,000 infants per year in the United States (Siddiq et al., 2020). Abnormal morphogenesis, environmental factors, and inflammatory dysregulation contribute to the development of biliary atresia, triggering a proinflammatory response that targets duct epithelium injury to produce severe cholangiopathy (Asai et al., 2015). There are several experimental systems of biliary atresia, including toxin-induced bile duct injury model in lambs and calves or zebrafish (Harper et al., 1990); programmed atresia model of sea lampreys (Cai et al., 2013); and rhesus rotavirus type A infection model. In addition, it has been found that intrahepatic injection of chemicals such as carbon tetrachloride, ethanol, or formalin can activate an inflammatory response similar to biliary atresia in an adult rat model (Tatekawa et al., 2013; Dumont et al., 1996). The cause and

This study was supported by the National Natural Science Foundation of China [Grant 81804142], the China Postdoctoral Science Foundation [Grant 2020M670026ZX], and the Chinese Medicine Scientific Research Special Project of Henan Province [Grant 2017JDZX035].
[1]J.-L.Q. and G.-F.Z. contributed equally to this work.
dx.doi.org/10.1124/jpet.121.001020.

ABBREVIATIONS: ALT, alanine aminotransferase; AST, aspartate aminotransferase; IHC, immunohistochemistry; miRNA, microRNA; α-SMA, α-smooth muscle actin; TEM, transmission electron microscopy; TGF-β, transforming growth factor-β.

pathogenesis of biliary atresia are still not fully understood. We tried to investigate factors contributing to the progression of liver fibrosis during biliary atresia and identify inflammatory pathways that can be targeted as therapeutic targets for liver fibrosis.

Transforming growth factor-β (TGF-β) plays a pivotal role in liver physiology and pathology from simple liver injury to fibrosis, cirrhosis, and even cancer (Fabregat and Caballero-Diaz, 2018). TGF-β/Smad signaling is a key mediator in the progression of fibrosis and inflammation. Upon dimeric ligands binding, TGF-β type II receptor (TβR2) recruits type I receptor to assemble into heteromeric kinases complex and phosphorylates the Gly-Ser–rich domain of type I receptor and induces a conformational change. Activated type I receptor subsequently phosphorylates Ser-Ser-X-Ser motif at the carboxy-terminal end of the receptor-regulated Smads (R-Smads), such as Smad2 and Smad3. Phosphorylated Smad2 and Smad3 form heterocomplexes with one common Smad (co-Smad), Smad4, and translocate into the nucleus (Hata and Chen, 2016). Together with other cofactors, they regulate the transcription of multiple target genes (e.g., type I collagen, α-smooth muscle actin [α-SMA], and Snail), finally presenting many biologic functions (Wei et al., 2013). On the contrary, as inhibitory Smads, Smad6 and Smad7 can antagonize the R-Smads and co-Smad mediated signaling by inhibiting the phosphorylation of R-Smads and promote the degradation of receptor complexes (Moustakas et al., 2001).

MicroRNAs (miRNAs) are involved in virtually every cellular biological process including cell proliferation, development, differentiation, immunity, fibrosis and carcinogenesis (O'Brien et al., 2018). Many miRNAs are estimated to regulate the activation of hepatic stellate cell (HSC) and liver fibrosis by modulating TGF-β/SMAD signaling. Several miRNAs are classified as antifibrotic such as miR-106b, miR-146a, miR-204-5p, which targets TβR2, smad2/3 or smad4, respectively (Hata and Chen, 2016). Other miRNAs are classified as profibrogenic. miRNA-30, miRNA-212-3p and miRNA-17-5p are reported to modulate TGF-β signaling through targeting the Smad7 (Dewidar et al., 2019). Many studies have revealed the epigenetic regulation of miR-145 on TGF-β/Smad signaling (Zhou et al., 2016). We wonder if miR-145 can regulate liver fibrosis during biliary atresia.

Ligustrazine, an effective bioactive component of Ligusticum chuanxiong Hort, is a herb widely used in China to treat cardiovascular disease (Zhang et al., 2018). Because of its excellent antifibrotic efficacy, ligustrazine has been on preclinical research for many years. Ligustrazine could alleviate and delayed the accumulation of myocardial collagen, and also has protective effects against pulmonary fibrosis induced by hyperoxia and bleomycin (Huang et al., 2018). Ligustrazine can attenuate renal tubulointerstitial fibrosis by restraining the epithelial-myofibroblast transition of tubular epithelial cells (Yuan et al., 2012). Recent studies reveal that ligustrazine improves liver histology and reduces fibrosis by downregulating inflammatory cytokines (Lu et al., 2016) or suppression on HSC activation (Zhang et al., 2014 and Zhang et al., 2012). Nevertheless, the mechanisms underlying ligustrazine in hepatic fibrosis are not fully elucidated.

In this study, we aim to study the therapeutic target for ligustrazine during liver fibrosis in ethanol-induced biliary atresia rat model and TGF-β–induced HSC activation cell model. We found that ligustrazine inhibited miR-145 activated TGF-β/smad signal pathway to protect against hepatic fibrosis. This study broadened the understanding of molecular mechanisms for ligustrazine involved in antifibrotic therapies.

Materials and Methods

Cells, Lentivirus, and Treatments. Rat HSC cell line HSC-T6 was purchased from Bioswamp Life Science (Wuhan, China) and cultured in Sulbecco's modified Eagle's medium (Hyclone, South Logan, UT) with 10% FBS (Gibco, Grand Island, NY). Cells were incubated in 5% CO_2 at 37°C. Lentivirus rLV, rLV-miR-145 and rLV-miR-145 sponge were purchased from Myhalic Biotechnological (Wuhan, China).

To study the effect of ligustrazine on TGF-β1–induced fibrosis, HSC-T6 cells were first treated with 2.5 ng/ml TGF-β1 and then with ligustrazine (2.5 μg/ml) for 24 or 48 hours. Cells were subjected to quantitative reverse-transcription polymerase chain reaction (RT-qPCR) and Western blotting.

To evaluate the infection efficiency of rLV, rLV-miR-145 and rLV-miR-145 sponge, as well as knockdown or overexpression of miR-145, HSC-T6 cells were infected with rLV, rLV-miR-145 and rLV-miR-145 sponge and cultured for 72 hours. The infection efficiency was determined by observing the fluorescence density under a microscope. The expression of miR-145 was determined using RT-qPCR.

To investigate whether miR-145 and SMAD3 were involved in the ligustrazine regulation of TGF-β1 induced fibrosis, HSC-T6 cells were first infected with rLV-miR-145 and rLV-miR-145 sponge, in the presence or absence of SMAD3 inhibitor SIS3 (5 μM), then treated with 2.5 ng/ml TGF-β1, and then with ligustrazine (2.5 μg/ml) for 48 hours. Cells were subjected to RT-qPCR, immunofluorescence and Western blotting.

Animals and Treatment. Outbred male Sprague-Dawley rats (weighing 200–250g) were purchased from Animal Experiment Center of Henan University of Chinese Medicine and housed in an specific-pathogen-free condition under a 12-hour light/dark cycle, with a room temperature of 22–26°C and humidity of 50–60%. All rats had free access to food and water ad libitum. All animal procedures were performed according to the national animal operation guideline and this study was reviewed and approved by the animal ethics committee of the First Affiliated Hospital of Henan University of Chinese Medicine.

Thirty rats were randomly assigned into five groups (n = 6 per group): control, sham, model, model plus pirfenidone, and model plus ligustrazine groups. Ethanol-induced biliary atresia rat model was developed as previously described (Ge et al., 2014; Tatekawa et al., 2013). In brief, laparotomy was performed through a midline incision. Next, we performed a ductotomy in the common bile duct above the confluence with the pancreatic duct using microsurgical techniques. Next, we inserted a 2 French silicon catheter (0.7 mm outer diameter and 19mm length) into the common bile duct, fixing with 6-0 nylon. During the operation, the biliary branches to the caudate and right lateral lobes were left intact, whereas the common bile duct was ligated distal to the cannulation site and divided. Then, we used a microsyringe to connect the catheter and injected saline (sham group) or pure ethanol into the catheter for about 30 second. We clamped the catheter for 5 minute and then released it. We inserted the opposite end of the catheter into the intestine, 3 cm distal to the ligament of Treitz, and fixed it with 11-0 nylon. One day after the operation, the animals were allowed food and water. Model rats then received saline (1 ml/100g/d), ligustrazine (10 mg/kg/d; L117992, HPLC $\geq$ 98%, Aladdin, Shanghai, China) or pirfenidone (300mg/kg/d; positive control; P129335, Aladdin) treatment by oral gavage daily for 14 days. Drug doses were determined according to the equivalent dose converted from the clinically effective dose for humans (Huang et al., 2004). Serum samples were collected from the posterior orbital venous plexus at 1, 3, 7, and 14 days after modeling and used for biochemical analysis. After treatment of 14 days, rats were anesthetized with sodium pentobarbital (40 mg/kg; P3761, Sigma-Aldrich, St Louis, MO) and killed through cervical dislocation. Liver tissues were collected and stained with H&E or Masson, or analyzed using immunohistochemistry

(IHC), transmission electron microscopy (TEM), RT-qPCR, and Western blotting.

Biochemical Analysis. Serum levels of total bilirubin, alanine aminotransferase (ALT), and aspartate aminotransferase (AST) were analyzed using BS-420 Biochemistry Analyzer (Mindray, Ltd., Guangdong, China).

H&E and Masson Staining. Collected tissues were fixed in 10% formaldehyde, embedded in paraffin, and cut into serial sections of 3-μm thickness, which were stained with H&E and Masson according to standard protocols. The slides were observed under a DM1000 light microscope (Leica, Wetzlar, Germany) and images were captured. We classified the histopathology of liver samples for fibrosis stage as 5-point scale according to a previous report (Dong et al., 2017): 0, no fibrosis; 1, minimal fibrosis (portal fibrosis without septa); 2, mild fibrosis (portal fibrosis with few septa); 3, moderate fibrosis (numerous septa without cirrhosis); and 4, cirrhosis.

IHC. Tissue sections were first deparaffinized and rehydrated and then subjected to antigen retrieval. Then sections were subjected to quench endogenous peroxidase activity and blocked with 10% normal goat serum. Next, the sections were incubated with primary rabbit antibodies against TGF-β1 (Bioswamp, dilution 1:100), TβR2 (Abcam, Cambridge, MA, USA; dilution 1:100), phosphorylated (p)-SMAD2/3 (Abcam, dilution 1:50), SMAD4 (Novus, dilution 1:100), SMAD7 (Bioswamp, dilution 1:100), collagen I and α-SMA (Abcam, dilution 1:100) overnight at 4°C. Next the sections were incubated with MaxVision horseradish peroxidase (HRP)-Polymer anti-rabbit secondary antibodies (MXB, Fujian, China) and then stained with DAB and hematoxylin following the manufacturer's protocols. The sections were observed under a DM1000 light microscope (Leica) and images were captured.

RNA Extraction and RT-qPCR. Total RNA was extracted using TRIzol reagent following the manufacturer's protocols (Ambion, Thermo Fisher). cDNA was synthesized using PrimeScript II RTase kit (Bioscience, Shanghai, China). Quantitative PCR was performed using SYBR FAST qPCR Master Mix (KAPA Biosystems) on a CFX96 Real-Time PCR Detection System (Bio-Rad). GAPDH was used as housekeeping genes for data normalization. U6 was used as an internal control for miR-145. Gene-specific primer sequences are listed in Table 1.

Western Blotting. Cells or tissues were lysed using NP-40 lysis buffer containing 50 mM Tris pH 8.0, 150 mM NaCl, 1% NP-40, EDTA-free protease inhibitor cocktail (Roche). The lysates' protein concentrations were quantified using a BCA Protein Assay Kit (Bio-Rad). Protein samples were separated by SDS-PAGE and were transferred onto PVDF membranes (Millipore). After that, membranes were first blocked and then incubated with primary antibodies against TGF-β1 (Bioswamp, dilution 1:1000), TβR2 (Abcam, Cambridge, MA, USA; dilution 1:1000), SMAD2/3 (Abcam, dilution 1:1000), phosphorylated (p)-SMAD2/3 (Abcam, dilution 1:100), SMAD4 (Novus, dilution 1:1000), SMAD7 (Bioswamp, dilution 1:1000), collagen I (Abcam, dilution 1:2000), α-SMA (Abcam, dilution 1:2000) and GAPDH (Bioswamp, dilution 1:1000) at 4°C overnight, following incubation with horseradish-peroxidase-conjugated secondary antibodies. The membranes were treated with an Enhanced Chemiluminescence kit (ECL; Millipore) and ananlyzed using TANON GIS software under a Tanon5200 Imaging System (Tanon, Shanghai, China). GAPDH was used as an internal control.

TABLE 1
Primers used in the study

Primers	Sequence (5′-3′)	Fragment (bp)
mir-145-F	GGGGTCCAGTTTTCCCAG	60
mir-145-R	AACTGGTGTCGTGGAGTCGGC	
U6-F	CTCGCTTCGGCAGCACATATACT	93
U6-R	ACGCTTCACGAATTTGCGTGTC	
TβR2-F	TCCATCTGTGAGAAGCCGC	117
TβR2-R	CAGAGTGAAGCCGTGGTAGGT	
SMAD4-F	ATCACTATGAGCGGGTTGT	168
SMAD 4-R	TTGGTGGATGTTGGATGG	
SMAD 7-F	GTGCGTGGTGGCATACTGG	170
SMAD 7-R	CGATCTTGCTCCTCACTTTCTG	
Collagen I-F	GCCTAGCAACATGCCAATC	202
Collagen I-R	GCAGCAAAGTTCCCAGTAAGA	
alpha-SMA-F	CCTGAAGTATCCGATAGAACACG	275
alpha-SMA-R	CATCTCCAGAGTCCAGCACAA	
GAPDH-F	CAAGTTCAACGGCACAG	138
GAPDH-R	CCAGTAGACTCCACGACAT	

Immunofluorescence and Confocal Microscopy. Cells were fixed with 4% formaldehyde, permeabilized with 0.1% Triton X-100, and blocked with PBS containing 5% normal serum and 0.3% Triton X-100. Subsequently, cells were incubated with diluted specific primary antibodies overnight at 4°C and then fluorochrome-conjugated secondary antibodies for 1 hour. Next, 4′,6-diamidino-2-phenylindole was used to stain the nuclei. Finally, the cells were subjected to microscopic analysis on an Olympus FluoView FV1000 confocal laser microscope under a 60× oil objective.

TEM. Samples were fixed in 2.5% glutaraldehyde at 4°C for 30 minutes and then fixed in 1% osmic acid for 1 hour. The samples were then dehydrated and embedded in araldite. The specimens were placed at 60°C for polymerization. Using ultramicrotome, ultrathin sections (100 nm) were prepared, which were picked up on uncoated copper grids. Sections were then stained with uranyl acetate and lead citrate. Finally, the stained sections were observed under a HT7700 (Hitachi, Tokyo, Japan). TEM and images were photographed.

Statistical Analysis. Statistical analysis was performed using GraphPad Prism (San Diego, CA). Data were representative of three independent experiments and are expressed as means ± SD. Comparison between groups was performed using one-way ANOVA followed by the Tukey post hoc test. A P value of less than 0.05 was considered statistically significant.

Results

Ligustrazine Alleviated Liver Pathology in Ethanol-Induced Biliary Atresia Model. First, the liver appearance was observed. As shown in Fig. 1A, the liver of five groups differed markedly in morphology. Gross appearance of the liver from the model group was yellowish and covered with small surface nodules, whereas ligustrazine and pirfenidone treatment rescued these pathologic changes. Next, cellular morphology of the liver was determined by TEM (Fig. 1B). Integrated nucleus, well-developed rough endoplasmic reticulum, and abundant mitochondria were observed in the control group and sham group, whereas significantly decreased rough endoplasmic reticulum and mitochondria and more lysosomes were found in the model group. Moreover, ligustrazine or pirfenidone treatment reversed these changes. Apart from morphologic observation, histologic and biochemical analyses were further performed to investigate the effect of ligustrazine on pathologic changes and progressions of the biliary atresia model. Representative H&E and Masson staining revealed severe liver fibrosis, increased necrosis, inflammation, and evident collagen accumulation of the liver tissues in the model group, as compared with control liver, and ligustrazine significantly ablated liver fibrosis and collagen deposition (Fig. 1, C–E). Moreover, we evaluated the clinical biochemical parameters of liver enzyme AST and ALT, and bilirubin metabolism total bilirubin levels in serum for the assessment of liver function. After ethanol injection in the model group, liver enzymes and bilirubin metabolism levels markedly increased, whereas intragastric administration of ligustrazine significantly inhibited AST and ALT levels at 14 days after operation, indicating that the ligustrazine greatly improved liver function (Fig. 1F). Collectively, these data demonstrated that

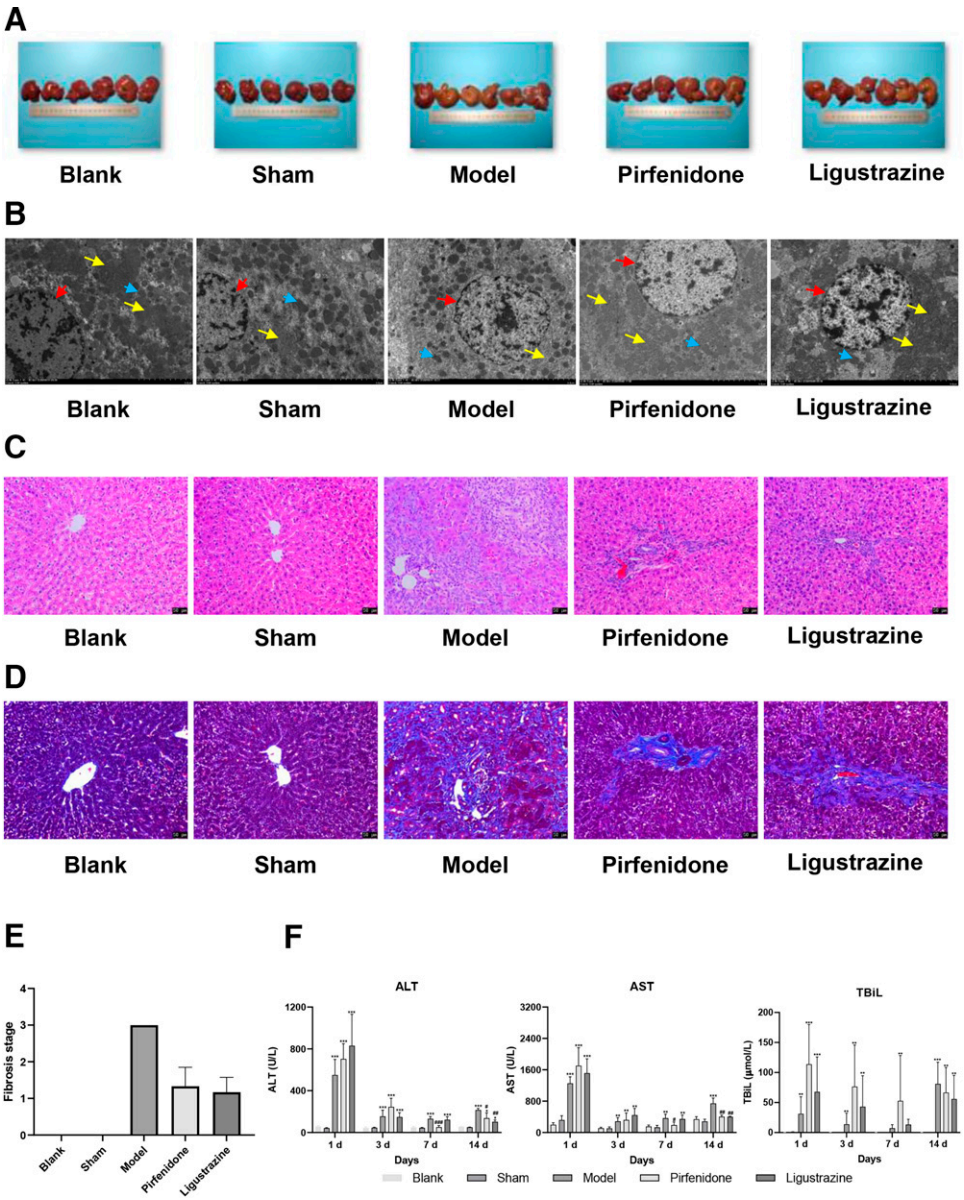

Fig. 1. Ligustrazine alleviated hepatic fibrosis in ethanol-induced biliary atresia rat model. The rats were divided into five groups as described in MATERIALS AND METHODS (n = 6 per group). Rats in the blank group received no surgery. Rats in the sham group underwent operation and had saline injected into their bile duct. Rats in the model, pirfenidone, and ligustrazine groups received a pure ethanol injection into their bile duct, followed by oral gavage administration of saline, pirfenidone, or ligustrazine respectively, for the next 14 days before subsequent liver extraction. (A) Gross appearance of the liver from each group (n = 6). The scale plate stands for 20 cm. (B) Electron micrographs of the livers of five groups (3,000×). Nucleus is indicated by a red arrow, rough ER a yellow arrow, and mitochondria a blue arrow. (C and D) Two weeks after operation, liver tissues were collected. Histologic analyses were performed by H&E (C) and Masson's trichrome staining (D). Scale bar = 50 μm. (E) Assessment of fibrosis stage according to the H&E and Masson staining. (F) Assessment of levels of liver enzymes, ALT and AST and bilirubin metabolism, TBiL in blood samples from experimental rats of each group at 1, 3, 7, and 14 days. TBiL, total bilirubin. $^{*}P < 0.05$, $^{**}P < 0.01$, $^{***}P < 0.001$ compared with the blank group; $^{\#}P < 0.05$, $^{\#\#}P < 0.01$, $^{\#\#\#}P < 0.001$ compared with the model group.

ligustrazine notably mitigated liver fibrosis in the ethanol-induced biliary atresia rat model.

Ligustrazine Suppressed Hepatic Fibrosis via Abating TGF-β/smads Signaling. Then we investigated whether the TGF-β/smads pathway was involved in the ligustrazine-regulated liver fibrosis. The mRNA levels of collagen I, α-SMA, and related proteins in the liver tissues were assessed. The data showed that ligustrazine largely repressed the upregulation of collagen I and α-SMA in the biliary atresia model and had no effect on improved TβR2, SMAD4, and SMAD7 mRNA levels (Fig. 2A). However, levels of these proteins showed different results. Ligustrazine significantly decreased the upregulated collagen I, α-SMA, TβR2, SMAD4, and SMAD7 protein levels and the phosphorylation of SMAD2 and SMAD3 (Fig. 2B). Similar results were obtained by IHC assays (Fig. 2C).

We also examined the protein and mRNA level changes of these proteins in cells. As shown in Fig. 3, the results indicated that TGF-β challenge raises α-SMA mRNA and protein levels compared with the control at both 24 and 48 hours, and ligustrazine treatment remarkably downregulated α-SMA expression. In accordance with this, ligustrazine treatment also reduced TGF-β–induced phosphorylation of SMAD 2 and SMAD3 at both 24 and 48 hours (Fig. 3).

Taken together, our data suggested that ligustrazine interfered with the TGF-β/smads signaling to alleviate hepatic fibrosis.

Ligustrazine Increased the Expression of miR-145. miR-145-5p is reported to target and reduce the expression of SMAD2/3, thus arresting the development of fibrogenesis and decreasing hypertrophic scar formation (Xu et al., 2019; Shen et al., 2020). We wonder whether miR-145 was involved in the mediation of ligustrazine-regulated liver fibrosis. We found that in the model group, miR-145 expression was downregulated, and this upregulation was inhibited by ligustrazine administration (Fig. 4A). HSC cells also showed similar results (Fig. 4B). To further investigate the interplay of miR-145 in hepatic stellate cell activation, recombinant lentivirus rLV-miR-145 for

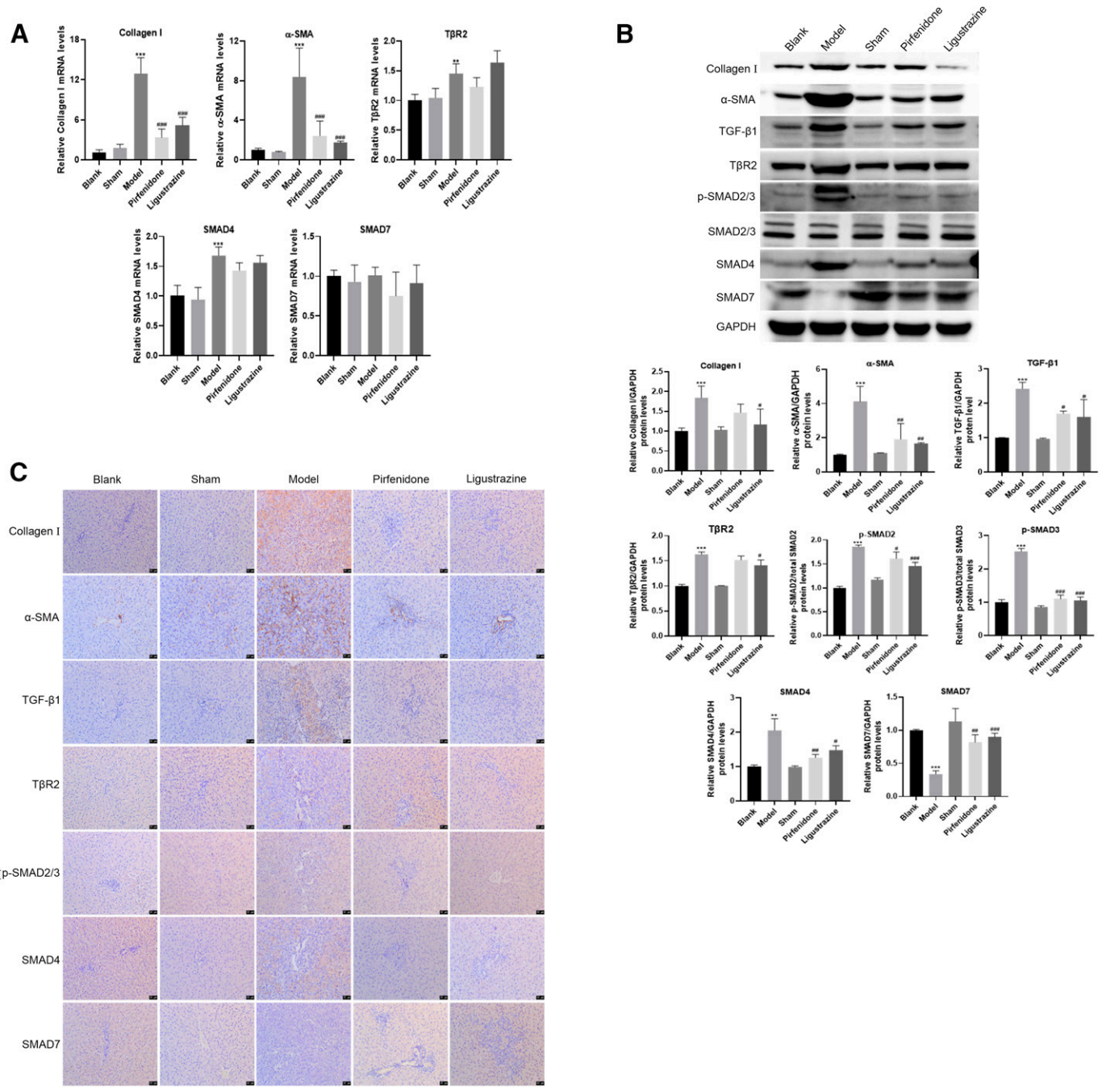

Fig. 2. Ligustrazine inhibited liver fibrosis via TGF-β/smad signaling. (A) Rat liver samples were isolated 14 days after surgery. RNA was extracted and subjected to qRT-PCR analysis. (B) Representative images of TGFβ1, TβR2, p-Smad2/3, total-Smad4, Smad7, Collagen Il and α-SMA expression detected using Western blotting. The data were quantitative of three independent experiments and are presented as mean ± S.D. (C) Representative images of TGFβ1, TβR2, p-Smad2/3, total-Smad4, Smad7, Collagen I, and α-SMA expression detected using IHC. Scale bar = 50 μm. $^{*}P < 0.05$, $^{**}P < 0.01$, $^{***}P < 0.001$ compared with the blank group; $^{\#}P < 0.05$, $^{\#\#}P < 0.01$, $^{\#\#\#}P < 0.001$ compared with the model group.

miR-145 overexpression and rLV-miR-145 sponge for miR-145 knockdown were used. We first detected the overexpression and knockdown efficiency of rLV-miR-145 and rLV-miR-145 sponge. HSC cells were infected with rLV-miR-145 or rLV-miR-145 sponge. Green fluorescent protein expression level showed a high degree of infection was achieved (Fig. 4C). The miR-145 RNA level was significantly increased in rLV-miR-155–infected cells and decreased in rLV-miR-145 sponge–infected cells compared with those infected with control rLV (Fig. 4D), indicating the overexpression and knockdown efficiency of rLV-miR 145 and rLV-miR 145 sponge.

Ligustrazine Blocked miR-145–Induced TGF-β/SMAD Signaling Activation. Then we investigated how miR-145 was involved in the ligustrazine regulation of TGF-β/SMAD signaling pathway in TGF-β–induced HSC activation and fibrosis. We first detected the expression of fibrotic marker α-SMA in each group using IFA. As shown in Fig. 5A, the control group with TGF-β treatment exhibited increased α-SMA

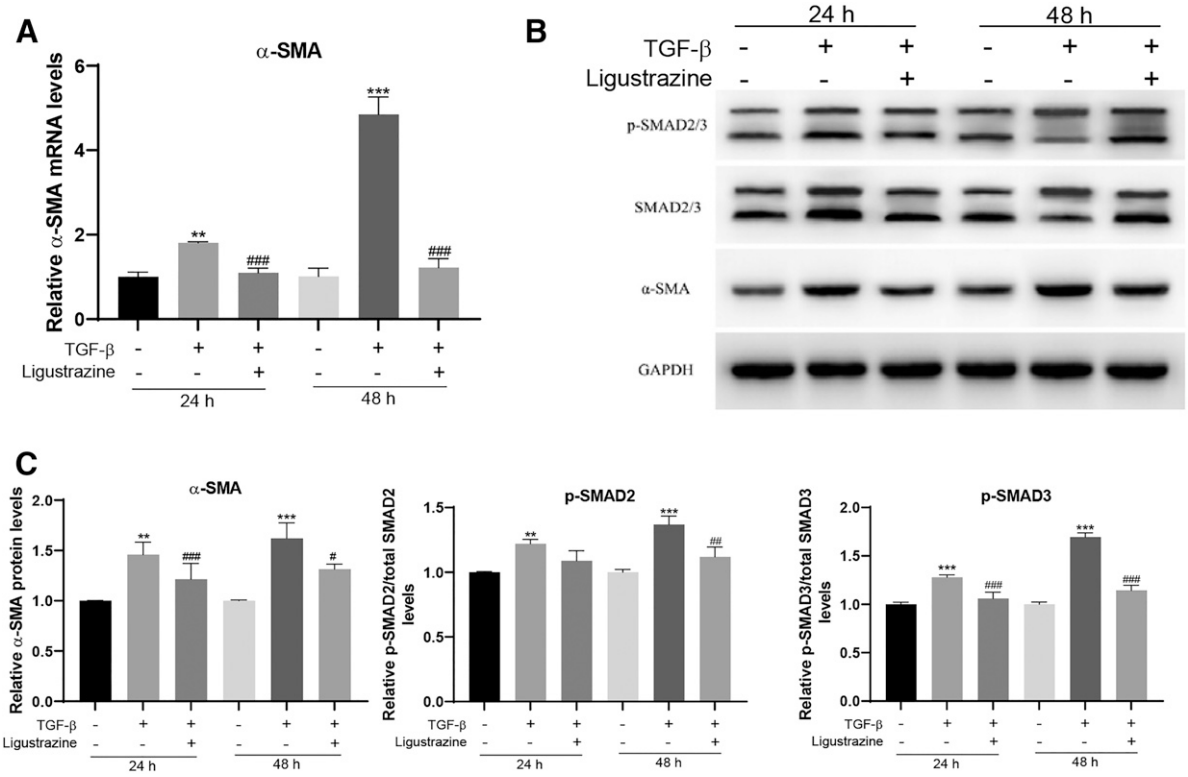

Fig. 3. Ligustrazine attenuated TGF-β induced HSC activation. (A and B) HSC cells were left untreated or treated with TGF-β1 for 24 or 48 hours with or without addition of ligustrazine. Cells were lysed and subjected to qRT-PCR (A) or Western blotting (B). (C) Quantitative analysis of B. The data are representative of three independent experiments and are presented as mean ± SD. $^{*}P < 0.05$, $^{**}P < 0.01$, $^{***}P < 0.001$ compared with the blank group; $^{\#}P < 0.05$, $^{\#\#}P < 0.01$, $^{\#\#\#}P < 0.001$ compared with the TGF-β1 treatment group.

distribution in comparison with the blank group; the rLV-miR 145 group showed decreased α-SMA, whereas the rLV-miR 145 sponge group showed even higher expression of α-SMA compared with the control group; and the ligustrazine group revealed similar expression of α-SMA compared with the SIS3 group. These results provided evidence that miR-145 promoted hepatic fibrosis and ligustrazine acted as a miR-145 suppressor. In line with the IFA results, RNA and protein levels of α-SMA and another fibrotic marker collagen I were quantified by RT-qPCR and Western blot analyses. Both showed similar changes (Fig. 5, B and C). In addition, the expression of molecules involved in the TGF-β signaling pathways was examined. TβR2, p-SMAD2/3, and SMAD 4 showed analogous alteration patterns by treatment of rLV-miR 145 sponge, ligustrazine, and smad3 inhibitor SIS3, whereas SMAD 7 caused an opposite effect. In conclusion, these data illustrated that ligustrazine restrained the miR-145 accelerated TGF-β/SMAD signaling and fibrosis process of HSC cells.

Discussion

In this study, we identified the antifibrotic function of ligustrazine on hepatic fibrosis in an ethanol-induced biliary atresia rat model. Pure ethanol injection induced bile duct injury and liver fibrosis in model rats. Morphologic observation and pathologic staining showed that ligustrazine ameliorated ethanol-caused liver impairment. Furthermore, we found that ligustrazine upregulated miR-145 expression and inhibited the TGF-β/SMAD signaling pathway both in vivo and in vitro. Moreover, overexpression and knockdown of miR-145 confirmed that miR-145 is involved in the ligustrazine inhibition of liver fibrosis through the TGF-β/SMAD signaling pathway.

The present study showed that ligustrazine inhibited biliary atresia-induced liver fibrosis through the TGF-β/SMAD signaling pathway. TGF-β plays an important role in liver pathology from simple liver injury to fibrosis, cirrhosis and even cancer (Fabregat and Caballero-Diaz, 2018). TGF-β/Smad signaling is a key mediator in the progression of fibrosis and inflammation and therefore is always the therapeutic target of many drugs.

Protein expressions of proteins involved in the TGF-β/Smad signaling pathway are subject to various positive and negative posttranslational regulations that occur upon specific stimulation. Many studies have revealed that epigenetic regulation of miR-145 on TGF-β/Smad signaling (Zhou et al., 2016). Expression of miR-145-5p postpones the progression of fibrogenesis and inhibits the formation of hypertrophic scar by downregulating the Smad2/3 expression (Shen et al., 2020). miR145 can suppress TGF-β–dependent extracellular matrix accumulation and fibrosis by targeting TβR2 (Zhao et al., 2015). TGF-β family member, ACVRIB, was also identified as a miR-145 target (Yan et al., 2012). Apart from regulating TGF-β/Smad signaling for antifibrotic function, decreased miR-145 expression contributes to biliary atresia–induced liver fibrosis by targeting a membrane skeletal protein Adducin 3 (Ye et al., 2017). miRNA-145 can inhibit HSC activation and proliferation by targeting ZEB2, a key mediator of epithelial-to-mesenchymal transition. On the other hand, miR-145 has been implicated to have profibrogenic character. TGF-β–induced human subconjunctival fibrosis is mediated by miR-145. miR-145 deficiency

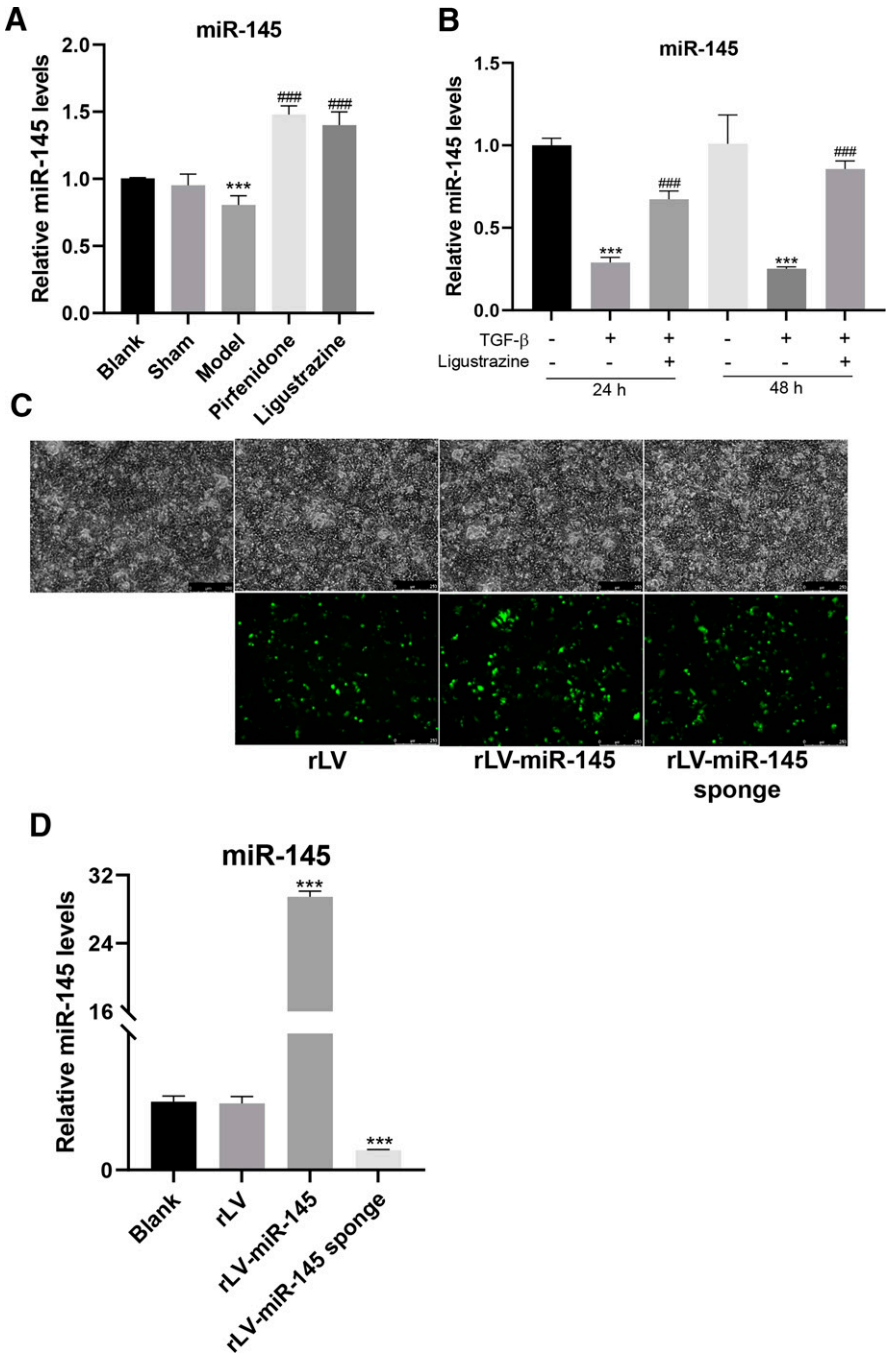

Fig. 4. MiR-145 expression was altered by ligustrazine and validation of miR-145 overexpression and knockdown by recombinant lentivirus. (A) Liver tissues were harvested 14 days after ethanol-induced biliary atresia rat model establishment. miR-145 RNA levels in the liver samples of the five groups were quantified using qRT-PCR assays. (B) HSC cells were challenged with or without TGF-β1 for 24 or 48 hours and treated with ligustrazine. Cells were subjected to qRT-PCR analysis for miR-145 expression. $^{*}P < 0.05$, $^{**}P < 0.01$, $^{***}P < 0.001$ compared with the blank group; $^{\#}P < 0.05$, $^{\#\#}P < 0.01$, $^{\#\#\#}P < 0.001$ compared with the TGF-β1 treatment group. (C) HSC cells was infected with rLV, rLV-miR-145 and rLV-miR-145 sponge, and the green fluorescent protein (green) expressed were imaged with a fluorescence microscope. (D) qRT-PCR was performed to quantify the expression level of miR-145 in rLV, rLV-miR-145– and rLV-miR-145 sponge–infected HSC cells for evaluation of miR-145 overexpression and knockdown efficiency. The data are representative of three independent experiments and are presented as mean ± S.D. $^{***}P < 0.001$ compared with the rLV group

attenuates bleomycin-induced pulmonary fibrosis (Yang et al., 2013). miR-145 promotes the activation of HSC and liver fibrosis by targeting a regulator of α-SMA transcription Krüppel-like factor 4 (Men et al., 2017). In contrast, our data demonstrated that miR-145 inhibited collagen accumulation and HSC activation. The proper explanation of the opposite outcomes of miR-145 in fibrosis progression might be crosstalk of multiple cellular signaling pathways involving miR-145, and in a tissue-specific manner.

In this study, pirfenidone was used as a positive control. Pirfenidone is an antifibrotic drug that has been approved for treating patients with idiopathic pulmonary fibrosis (Shah et al., 2021). Its possible application in other diseases including heart failure with preserved ejection fraction (Graziani et al., 2021), nonalcoholic steatohepatitis (Komiya et al., 2017), and advanced liver fibrosis (Poo et al., 2020) has also been investigated. Pirfenidone functions against fibrosis by targeting the TGF-β signaling pathway (Li., et al., 2021). Recently, pirfenidone was reported to alleviate choroidal neovascular fibrosis through the TGF-β/smad signaling pathway (Gao et al., 2021). The present study also showed that both ligustrazine and pirfenidone alleviate liver fibrosis through the TGF-β/SMAD signaling pathway in the biliary atresia model, suggesting that ligustrazine and pirfenidone may share a similar molecular mechanism. In the preparation of this manuscript, TGF-β2 was reported to be involved in biliary-derived liver diseases

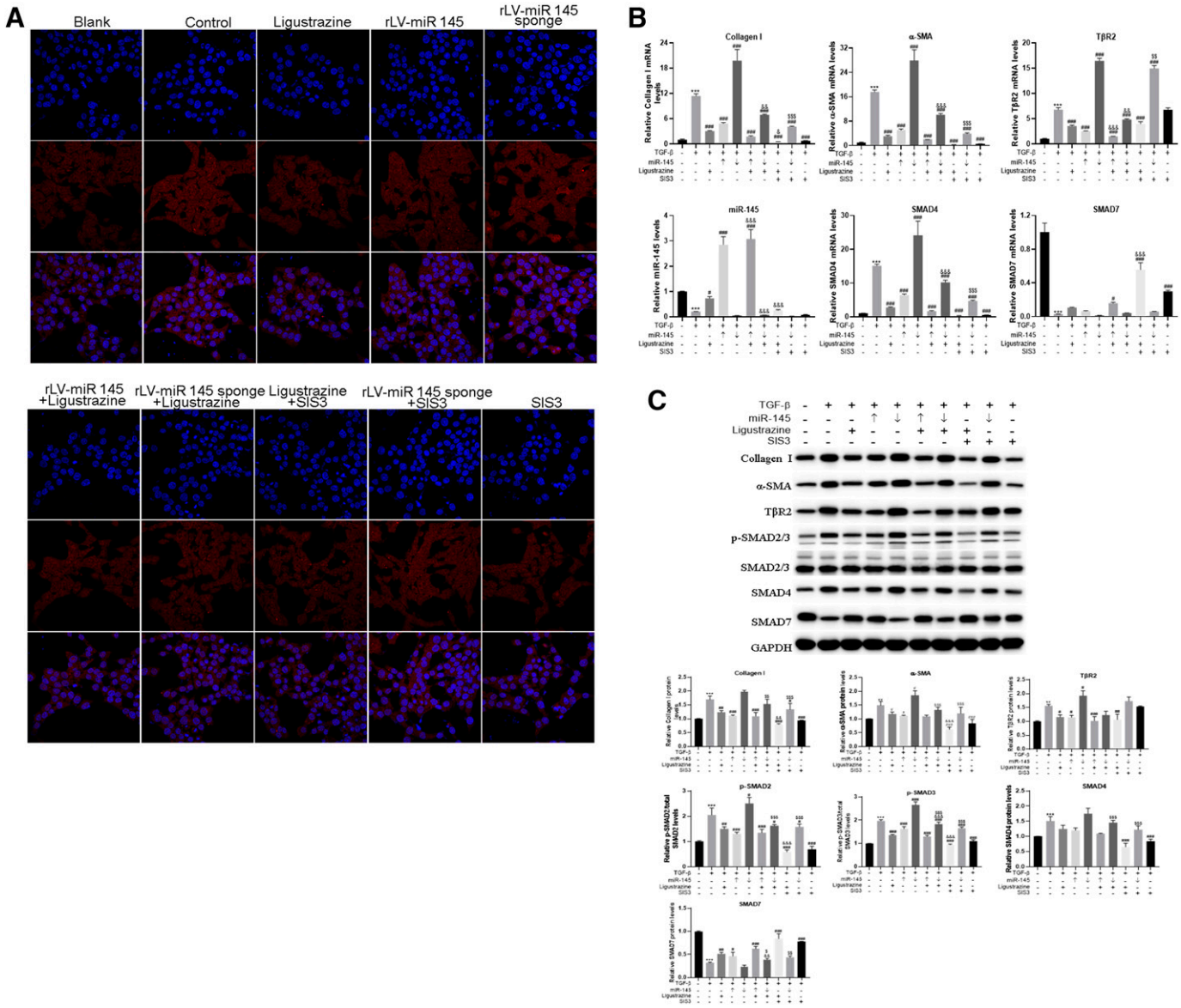

Fig. 5. Ligustrazine blocked miR-145–induced TGF-β/SMAD signaling activation. (A) HSC cells were stimulated as indicated in the figure. Immunofluorescence was performed using α-SMA antibody (red). Nuclei were stained with 4′,6-diamidino-2-phenylindole (blue). (B) The RNA levels of miR-145 and TGF-β/SMAD signaling molecules TβR2, Smad4, Smad7, and fibrosis markers Collagen I and α-SMA in each group were evaluated using qRT-PCR assay. (C) HSC cells in the 10 groups were lysed and subjected to Western blot analysis for TGF-βR2, p-Smad2/3, total Smad2/3, Smad4, Smad7, Collagen I, and α-SMA protein expression levels. The quantitative data are from three independent experiments and are presented as mean ± S.D. $^{*}P < 0.05$, $^{**}P < 0.01$, $^{***}P < 0.001$ compared with the blank group; $^{\#}P < 0.05$, $^{\#\#}P < 0.01$, $^{\#\#\#}P < 0.001$ compared with the TGF-β1 treatment group; $^{\&}P < 0.05$, $^{\&\&}P < 0.01$, $^{\&\&\&}P < 0.001$ compared with the TGF-β1 + ligustrazine treatment group; $^{\$}P < 0.05$, $^{\$\$}P < 0.01$, $^{\$\$}P < 0.001$ compared with the TGF-β1 + miR-145 knockdown treatment group.

(Dropmann et al., 2020). Further studies are needed to investigate whether TGF-β2 is involved in the function of miR-145 in the present study.

Previous studies have reported that miR-199a, miR-33a, and miR-21 can enhance liver fibrosis while miR-200a, miR-454, and miR-146a can inhibit liver fibrosis through the TGF-β/SMAD signaling pathway (Xu et al., 2016). miR-199a and miR-200a target SMAD3, miR-454 and miR-146 target SMA4, and miR-33a and miR-21 target SMAD7. Ligustrazine sequesters liver fibrosis via participating miR-145–mediated inhibition of TGF-β/smads signal conduction. However, the precise mechanisms remain to be explored. Whether ligustrazine directly interacts with pathway molecules such as Smad2 or Smad3 or impacts the posttranscription modulation of Smads protein by ubiquitination, methylation or other processes, needs to be further investigated. As for miR-145, how ligustrazine influences canonical or noncanonical biosynthesis pathways of miR-145 in a direct or consensual way. Apoptosis is a potentially important pathogenic mechanism in the development of tissue fibrosis. Ligustrazine was identified to contribute to apoptotic death and tumor regression in human breast cancer in both in vitro and in vivo models (Pan et al., 2015). Ligustrazine was also reported to induce the apoptosis of colorectal cancer cells via p53-dependent mitochondrial pathway (Bian et al., 2021). Thus, ligustrazine might function to mitigate hepatic fibrosis through the apoptosis pathway.

Previous studies have confirmed the antifibrotic effect of ligustrazine in many fibrotic diseases (Yuan et al., 2012;

Zhang et al., 2012; Zhang et al., 2014; Lu et al., 2016; Huang et al., 2018; Zhang et al., 2018). The present study further confirmed that ligustrazine inhibited hepatic fibrosis by inhibiting miR-145–activated TGF-β/smad signal pathway, which broadened our understanding of the molecular mechanisms for the antifibrotic effect of ligustrazine.

In summary, we reported the essential role of ligustrazine in miR-145–controlled TGF-β/smads pathway, implying the clinical value of ligustrazine in therapies for liver fibrosis in patients with biliary atresia. It should be noted that the present study was performed in the adult rat model. The results should be further confirmed in a neonatal rat model. Moreover, liver fibrosis in the present biliary atresia model does not alter the pathogenesis of liver disease, indicating the therapeutic effect of ligustrazine in liver fibrosis with different causes. Therefore, more future research is needed to confirm the antifibrotic effect of ligustrazine in other liver fibrosis models and accurately address its molecular mechanisms before it can be applied to the clinic.

Authorship Contributions

Participated in research design: Qiu, Zhang, Duan, Chen.

Conducted experiments: Chai, Han.

Performed data analysis: Zheng, Li.

Wrote or contributed to the writing of the manuscript: Qiu, Duan, Chen.

References

Asai A, Miethke A, and Bezerra JA (2015) Pathogenesis of biliary atresia: defining biology to understand clinical phenotypes. *Nat Rev Gastroenterol Hepatol* **12**:342–352.

Bian Y, Yang L, Sheng W, Li Z, Xu Y, Li W, and Zeng L (2021) Ligustrazine induces the colorectal cancer cells apoptosis via p53-dependent mitochondrial pathway and cell cycle arrest at the G0/G1 phase. *Ann Palliat Med* **10**:1578–1588.

Cai SY, Lionarons DA, Hagey L, Soroka CJ, Mennone A, and Boyer JL (2013) Adult sea lamprey tolerates biliary atresia by altering bile salt composition and renal excretion. *Hepatology* **57**:2418–2426.

Dewidar B, Meyer C, Dooley S, and Meindl-Beinker AN (2019) TGF-β in hepatic stellate cell activation and liver fibrogenesis-updated 2019. *Cells* **8**:1419.

Dong R, Yang Y, Shen Z, Zheng C, Jin Z, Huang Y, Zhang Z, Zheng S, and Chen G (2017) Forkhead box A3 attenuated the progression of fibrosis in a rat model of biliary atresia. *Cell Death Dis* **8**:e2719.

Dropmann A, Dooley S, Dewidar B, Hammad S, Dediulia T, Werle J, Hartwig V, Ghafoory S, Woelfl S, Korhonen H, et al. (2020) TGF-β2 silencing to target biliary-derived liver diseases. *Gut* **69**:1677–1690.

Dumont M, D'Hont C, Moreau A, Mbape H, Feldmann G, and Erlinger S (1996) Retrograde injections of formaldehyde into the biliary tree induce alterations of biliary epithelial function in rats. *Hepatology* **24**:1217–1223.

Fabregat I and Caballero-Díaz D (2018) Transforming growth factor-β-induced cell plasticity in liver fibrosis and hepatocarcinogenesis. *Front Oncol* **8**:357.

Ge JT, Li L, Wei YD, Wang HB, Qiao GL, Zhang Z, Liu Y, Ming AX (2014) Injection of ethanol into the common bile duct to establish a rat model of biliary atresia. *Acta Laboratorium Animalis Scientia Sinica* 50–52.

Graziani F, Lillo R, and Crea F (2021) Rationale for the use of pirfenidone in heart failure with preserved ejection fraction. *Front Cardiovasc Med* **8**:678530.

Gao C, Cao X, Huang L, Bao Y, Li T, Di Y, Wu L, and Song Y (2021) Pirfenidone alleviates choroidal neovascular fibrosis through the TGF-β/Smad signaling pathway. *J Ophthalmol* **2021**:8846708.

Govindarajan KK (2016) Biliary atresia: where do we stand now? *World J Hepatol* **8**:1593–1601.

Hata A and Chen YG (2016) TGF-β signaling from receptors to Smads. *Cold Spring Harb Perspect Biol* **8**:a022061.

Harper P, Plant JW, and Unger DB (1990) Congenital biliary atresia and jaundice in lambs and calves. *Aust Vet J* **67**:18–22.

Huang C, Wu X, Wang S, Wang W, Guo F, Chen Y, Pan B, Zhang M, and Fan X (2018) Combination of *Salvia miltiorrhiza* and ligustrazine attenuates bleomycin-induced pulmonary fibrosis in rats via modulating TNF-α and TGF-β. *Chin Med* **13**:36.

Huang J, Huang X, Chen Z, Zheng Q, and Sun R (2004) Conversion of equivalent doses between animals and between animals and humans in pharmacological tests [in Chinese]. *Chinese J Pharmacol Toxicol* **9**:1069–1072.

Komiya C, Tanaka M, Tsuchiya K, Shimazu N, Mori K, Furuke S, Miyachi Y, Shiba K, Yamaguchi S, Ikeda K, et al. (2017) Antifibrotic effect of pirfenidone in a mouse model of human nonalcoholic steatohepatitis. *Sci Rep* **7**:.

Li X, Ding Z, Wu Z, Xu Y, Yao H, and Lin K (2021) Targeting the TGF-β signaling pathway for fibrosis therapy: a patent review (2015-2020). *Expert Opin Ther Pat* **31**:723–743.

Lu C, Xu W, Zhang F, Shao J, and Zheng S (2016) Nrf2 knockdown attenuates the ameliorative effects of ligustrazine on hepatic fibrosis by targeting hepatic stellate cell transdifferentiation. *Toxicology* **365**:35–47.

Men R, Wen M, Zhao M, Dan X, Yang Z, Wu W, Wang MH, Liu X, and Yang L (2017) MircoRNA-145 promotes activation of hepatic stellate cells via targeting krüppel-like factor 4. *Sci Rep* **7**:40468.

Moustakas A, Souchelnytskyi S, and Heldin CH (2001) Smad regulation in TGF-beta signal transduction. *J Cell Sci* **114**:4359–4369.

O'Brien J, Hayder H, Zayed Y, and Peng C (2018) Overview of microRNA biogenesis, mechanisms of actions, and circulation. *Front Endocrinol (Lausanne)* **9**:402.

Poo JL, Torre A, Aguilar-Ramírez JR, Cruz M, Mejía-Cuán L, Cerda E, Velázquez A, Patiño A, Ramírez-Castillo C, Cisneros L, et al. (2020) Benefits of prolonged-release pirfenidone plus standard of care treatment in patients with advanced liver fibrosis: PROMETEO study. *Hepatol Int* **14**:817–827.

Pan J, Shang JF, Jiang GQ, and Yang ZX (2015) Ligustrazine induces apoptosis of breast cancer cells in vitro and in vivo. *J Cancer Res Ther* **11**:454–458.

Shah PV, Balani P, Lopez AR, Nobleza CMN, Siddiqui M, and Khan S (2021) A review of pirfenidone as an anti-fibrotic in idiopathic pulmonary fibrosis and its probable role in other diseases. *Cureus* **13**:e12482.

Shen W, Wang Y, Wang D, Zhou H, Zhang H, and Li L (2020) miR-145-5p attenuates hypertrophic scar via reducing Smad2/Smad3 expression. *Biochem Biophys Res Commun* **521**:1042–1048.

Siddiq S, Jimenez-Rivera C, Kuenzig ME, Lima I, Geraghty MT, Ng VL, Tam K, and Benchimol EI (2020) Direct health care costs, health services utilization, and outcomes of biliary atresia: a population-based cohort study. *J Pediatr Gastroenterol Nutr* **70**:436–443.

Tatekawa Y, Nakada A, and Nakamura T (2013) Intrahepatic biliary ablation with pure ethanol: an experimental model of biliary atresia. *Surg Today* **43**:661–669.

Wei X, Xia Y, Li F, Tang Y, Nie J, Liu Y, Zhou Z, Zhang H, and Hou FF (2013) Kindlin-2 mediates activation of TGF-β/Smad signaling and renal fibrosis. *J Am Soc Nephrol* **24**:1387–1398.

Xu T, Wu YX, Sun JX, Wang FC, Cui ZQ, and Xu XH (2019) The role of miR-145 in promoting the fibrosis of pulmonary fibroblasts. *J Biol Regul Homeost Agents* **33**:1337–1345.

Xu F, Liu C, Zhou D, and Zhang L (2016) TGF-β/SMAD pathway and its regulation in hepatic fibrosis. *J Histochem Cytochem* **64**:157–167.

Yuan XP, Liu LS, Fu Q, and Wang CX (2012) Effects of ligustrazine on ureteral obstruction-induced renal tubulointerstitial fibrosis. *Phytother Res* **26**:697–703.

Yan G, Zhang L, Fang T, Zhang Q, Wu S, Jiang Y, Sun H, and Hu Y (2012) MicroRNA-145 suppresses mouse granulosa cell proliferation by targeting activin receptor IB. *FEBS Lett* **586**:3263–3270.

Ye Y, Li Z, Feng Q, Chen Z, Wu Z, Wang J, Ye X, Zhang D, Liu L, Gao W, et al. (2017) Downregulation of microRNA-145 may contribute to liver fibrosis in biliary atresia by targeting ADD3. *PLoS One* **12**:e0180896.

Yang S, Cui H, Xie N, Icyuz M, Banerjee S, Antony VB, Abraham E, Thannickal VJ, and Liu G (2013) miR-145 regulates myofibroblast differentiation and lung fibrosis. *FASEB J* **27**:2382–2391.

Zhou DD, Wang X, Wang Y, Xiang XJ, Liang ZC, Zhou Y, Xu A, Bi CH, and Zhang L (2016) MicroRNA-145 inhibits hepatic stellate cell activation and proliferation by targeting ZEB2 through Wnt/β-catenin pathway. *Mol Immunol* **75**:151–160.

Zhang F, Lu S, He J, Jin H, Wang F, Wu L, Shao J, Chen A, and Zheng S (2018) Ligand activation of PPARγ by ligustrazine suppresses pericyte functions of hepatic stellate cells via SMRT-mediated transrepression of HIF-1α. *Theranostics* **8**:610–626.

Zhang X, Zhang F, Kong D, Wu X, Lian N, Chen L, Lu Y, and Zheng S (2014) Tetramethylpyrazine inhibits angiotensin II-induced activation of hepatic stellate cells associated with interference of platelet-derived growth factor β receptor pathways. *FEBS J* **281**:2754–2768.

Zhang F, Ni C, Kong D, Zhang X, Zhu X, Chen L, Lu Y, and Zheng S (2012) Ligustrazine attenuates oxidative stress-induced activation of hepatic stellate cells by interrupting platelet-derived growth factor-β receptor-mediated ERK and p38 pathways. *Toxicol Appl Pharmacol* **265**:51–60.

Zhao N, Koenig SN, Trask AJ, Lin CH, Hans CP, Garg V, and Lilly B (2015) MicroRNA miR145 regulates TGFBR2 expression and matrix synthesis in vascular smooth muscle cells. *Circ Res* **116**:23–34.

Address correspondence to: Fei Duan, Department of Gastroenterology, the First Affiliated Hospital of Henan University of Chinese Medicine, Zhengzhou, China. E-mail: kybduanfei@126.com; or Ling-Yan Chen, Department of Rehabilitation, The First Affiliated Hospital of Guangzhou Medical University, Guangzhou, China. E-mail: 125505219@qq.com